Anti-Sway Control of Container Cranes: Inclinometer, Observer, and State Feedback

Yong-Seok Kim, Keum-Shik Hong*, and Seung-Ki Sul

Abstract: In this paper, a novel anti-sway control system that uses an inclinometer as a sway sensor is investigated. The inclinometer, when compared with a vision system, is very cheap, durable, and easy to maintain, while providing almost the same performance. A number of observers to estimate the angular velocity of the load and the trolley velocity are presented. A state feedback controller with an integrator is designed. After a time-scale analysis, a 1/4-size pilot crane of a rail-mounted quayside crane was constructed. The performance of the proposed control system was verified with a real rubber-tired gantry crane at a container terminal as well as with the constructed pilot crane. Experimental results are provided.

Keywords: Crane control, modeling, observer, pendulum motion, state feedback, velocity profile.

1. INTRODUCTION

During the previous two decades, the endeavor to enhance the handling efficiency of containers at ports has pulled vigorous research in two directions: one is the fast movement of containers between a container ship and trucks [2,12-16,22,28], and the other is an automated container handling procedure in the yard [10,30-33]. There are two types of container cranes: a rail-mounted quayside crane (RMQC) and a rubber-tired gantry crane (RTGC). As the words imply, an RMQC transfers containers between a containership and trucks in the quay-side, and it can move on the rails located along the quay (see Fig. 1(a)). It is notable for its long outreach toward the sea-side, on which rails a trolley picking up containers from the ship and moving back and forth. Contrastingly, an RTGC handles containers in the container yard by moving them from one place to another or to trucks (see Fig. 8(a)).

When transferring a container, the swaying phenomenon of the container at the end of flexible ropes makes its positioning at an exact location very difficult. Because the fast loading/unloading of containers from/to a containership is most crucial, time-optimal control under zero terminal conditions has been widely investigated. However, there always exists a residual sway of the container at the end of a trolley stroke due to the unmodeled dynamics of the plant and to disturbances like wind. Related to the speed control method, an analytical solution of the time-optimal control for overhead cranes without a hoisting motion was investigated by Manson [22]. Sakawa and Shindo [28] classified the crane motion into five different sections and derived an optimal speed reference trajectory that minimizes a quadratic cost function, where the cost function was an integral of the weighted sum of the squares of the sway angle and its derivative. Auernig and Troger [2] investigated a time optimal control for diagonal movement using a simplified model. Hamalainen *et al.* [12] proposed an optimal path planning for a trolley crane, in which the path was split into five phases. In the works of Hong *et al*. [13,14], five velocity patterns for the trolley movement were derived and their traveling times were compared. Considering the length of this paper, however, detailed discussions related to time-optimal control are omitted and are instead referred to in the literature [2,12,14,22,23,28].

In contrast to speed control, the torque control method applies control forces/torques in such a way that the dynamics of the controlled system meet a given reference signal. The torque control method is more attractive from the aspects of accuracy and

Manuscript received July 2, 2004; accepted September 20, 2004. Recommended by Editor-in-Chief Myung Jin Chung. This work was supported by the Ministry of Science and Technology of Korea under a program of the National Research Laboratory, grant number NRL M1-0302-00-0039-03-J00-00-023-10.

Yong-Seok Kim is with the Advanced Technology Center, R&D Division for Hyundai & Kia Motors, 772-1 Jangduk-dong, Whasung-si, Gyunggi-Do 445-706, Korea (e-mail: glenn@hyundai-motor.com).

Keum-Shik Hong is with the School of Mechanical Engineering, Pusan National University, San 30 Jangjeon-dong, Gumjeong-gu, Busan 609-735, Korea (e-mail: kshong@pusan.ac.kr).

Seung-Ki Sul is with the School of Electrical Engineering and Computer Science, Seoul National University, ENG420-024 Kwanak P.O. Box 34, Seoul 151-744, Korea (e-mail: sulsk@plaza.snu.ac.kr).

* Corresponding author.

energy saving. Moustafa and Ebeid [24] investigated the nonlinear modeling and control of an overhead crane. Boustany and d'Andrea Novel investigated an indirect adaptive control using the dynamic feedback linearization and estimation technique in [4] and the nonlinear back-stepping control in [1]. Chung and Hauser [6] proposed a nonlinear controller to regulate the swing energy of the pendulum motion. Corriga et al. [7] proposed an implicit gain-scheduling controller, for which a linear parameter-varying model of the crane (according to changes in the length of the hoist rope) was utilized. In Hong *et al.* [16], to overcome the drawbacks of pre-determined reference control methods, a combination of time-optimal control and nonlinear residual sway control was proposed. Recently, an open loop control method, named input shaping control or command shaping control, was also applied to crane control by several researchers [17,27,30]. Unfortunately, due to the simplification of control models, the robustness of the designed controller also became an issue [3,5,8,18,21,29].

A crane is naturally an underactuated mechanical system, in which the number of actuators is less than the degree of freedom of the system. Specifically, assuming that the pendulum motion of the container is restricted to a plane, the degree of freedom of the crane is three, but the number of actuations is two, that is, trolley and hoist motors. For a given target position of the container, the trolley should travel as fast as possible. However, the fast trolley movement should not result in any residual sway of the container at the end of the transference. To achieve this, it is crucial to know the exact position of the container throughout the transference. The use of a vision system to measure the sway angle, through measuring the container position, has been actively investigated [15-17,23,33]. But, a vision system is very expensive and, furthermore, its long term maintenance is quite difficult.

In this paper, a new control strategy, not relying on a vision system, is investigated. The sway angle of the container was calculated from the information of the inclined angle of the spreader. Because an inclinometer is much cheaper and durable than a vision system, the use of an inclinometer, as a sway sensor, is the biggest advantage. Instead, the angular velocity of the container was estimated, because there is no direct way of calculating it from the inclination of the spreader. Three different observers to estimate the angular velocity are proposed: the first one uses the most simple model and trolley acceleration information; the second one uses a rather simple model and trolley force information; and the third one uses a nonlinear model and, therefore, is the most complicated. Among these, we need to choose one depending on available signals and the accuracy required.

The contributions of this paper are the following. A novel method for measuring the sway angle by using an inclinometer is proposed. This method utilizes the kinematics arising between the reeving structure and the spreader. Various observer designs are presented, which provide us the option to choose one. The state feedback control strategy using an integrator yields a simple control structure but one that is robust to model uncertainty. Finally, the developed algorithms are verified through a 1/4-scale pilot crane. The discussion on how to make a pilot crane via time-scale analysis is an additional contribution.

The paper is structured as follows: In Section 2, a control model is derived. In Section 3, an indirect measurement of the sway angle, by measuring the inclination of the spreader, is presented. In Section 4, various observers to estimate the sway angular velocity and trolley velocity are discussed. In Section 5, a state feedback control law using an integrator is designed. In Section 6, the experimental results are discussed. Conclusions are given in Section 7.

2. SYSTEM DYNAMICS

For the successful suppression of the sway motion of a suspended load, it is important to know what part of the crane dynamics should be included in the stage of control law design and what part should be

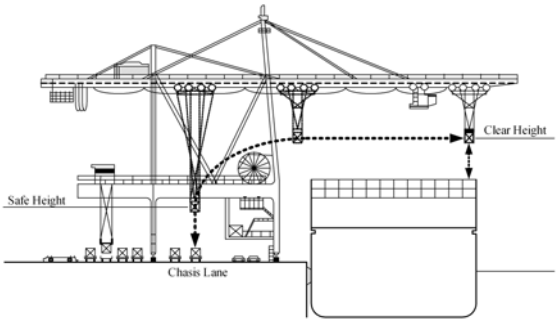

(a) Loading and unloading of containers.

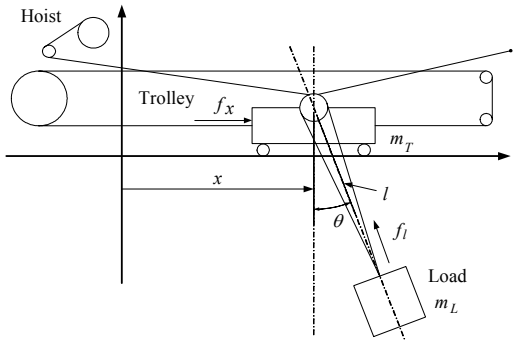

(b) Modeling: schematic for control system design.

Fig. 1. A typical rail-mounted quayside container crane system and its control model.

neglected. In the case of container cranes, in contrast to over-head cranes, a two-dimensional model is sufficient to represent the dynamics of the suspended load.

Fig. 1 illustrates a typical RMQC operating in a container terminal. The system consists of a trolley(s), a hoist(s), a spreader(s), and ropes. Typically, Fig. 1(a) represents a double-trolley system. The trolley, as shown in Fig. 1(b), is pulled to a desired position by the trolley rope, whereas the up and down movement of the load is accomplished by winding the hoist rope. The following assumptions are made: The trolley and the load, together, are regarded as a point mass moving in the vertical plane; all frictional elements in the trolley and hoist motions can be neglected; rope elongation is neglected.

In Fig. 1(b), the generalized coordinate q is defined as $q=[\theta,x,l]^T$, where θ is the sway angle, x is the trolley position, and l is the length of the suspended hoist rope, that is, from the sheave to the spreader. Then, the kinetic energy T and the potential energy V are given as follows:

$$\begin{aligned} T &= \frac{1}{2}m_T\dot{x}^2+\frac{1}{2}m_L(\dot{x}^2+\dot{l}^2+l^2\dot{\theta}^2 \\ &\quad +2\dot{x}\dot{l}\sin\theta+2\dot{x}l\dot{\theta}\cos\theta), \\ V &= -m_L g l\cos\theta, \end{aligned} \tag{1}$$

where m_T and m_L are the mass of the trolley and load, respectively, and g is the gravitational acceleration. Since the kinetic energy T is of the form $T(q,\dot{q})=\frac{1}{2}\dot{q}^T D(q)\dot{q}$, where $D(q)$ is a symmetric and positive definite matrix for $l > 0$ such that

$$D(q)=\begin{bmatrix} m_L l^2 & m_L l\cos\theta & 0 \\ m_L l\cos\theta & m_T+m_L & m_L\sin\theta \\ 0 & m_L\sin\theta & m_L \end{bmatrix}, \tag{2}$$

the following Euler-Lagrange equation can be used when deriving the equations of motion.

$$D(q)\ddot{q}+\left\{\frac{d}{dt}[D(q)]\dot{q}-\frac{\partial T(q,\dot{q})}{\partial q}\right\}+\frac{\partial V(q,\dot{q})}{\partial q}=Q. \tag{3}$$

Let the generalized force Q, associated with $q=[\theta,x,l]^T$, be $[0,f_x,f_y]^T$, where f_x and f_y are the forces applied to the trolley in the x-direction and to the suspended load in the l-direction, respectively. From (1)-(3), the equations of motion are

$$l\ddot{\theta}+2\dot{l}\dot{\theta}+g\sin\theta+\ddot{x}\cos\theta=0, \tag{4}$$

$$\begin{aligned} &(m_T+m_L)\ddot{x}+m_L l(\ddot{\theta}\cos\theta-\dot{\theta}^2\sin\theta) \\ &\quad +m_L\ddot{l}\sin\theta+2m_L\dot{l}\dot{\theta}\cos\theta=f_x, \end{aligned} \tag{5}$$

$$m_L\ddot{l}-m_L l\dot{\theta}^2-m_L g\cos\theta+m_L\ddot{x}\sin\theta=-f_l. \tag{6}$$

Now, to derive a linear time-invariant model, two things are further assumed: the sway angle is

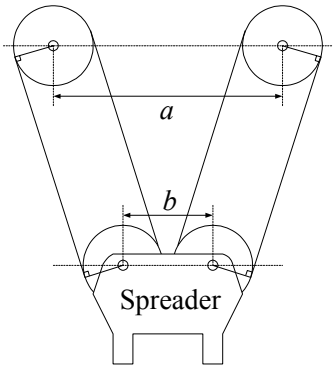

(a) The reeving structure of an RMQC.

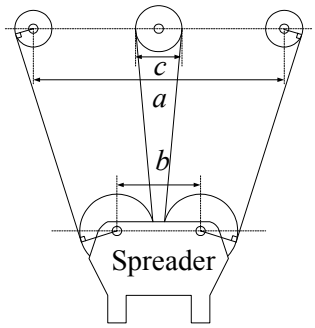

(b) The reeving structure of an RTGC.

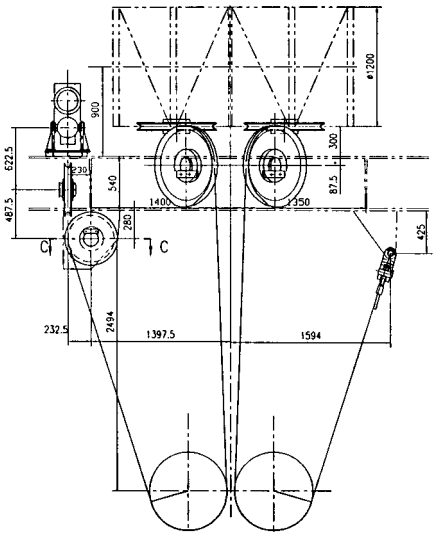

(c) A detailed drawing of (b): example.

Fig. 2. Hoist rope reeving structures.

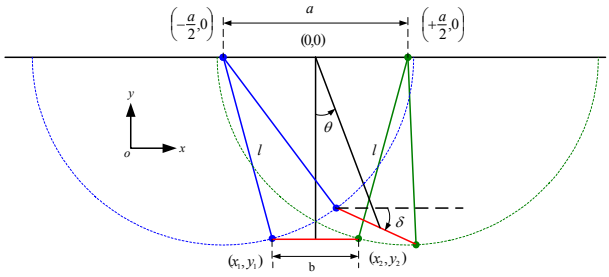

(a) RMQC (two-rope structure).

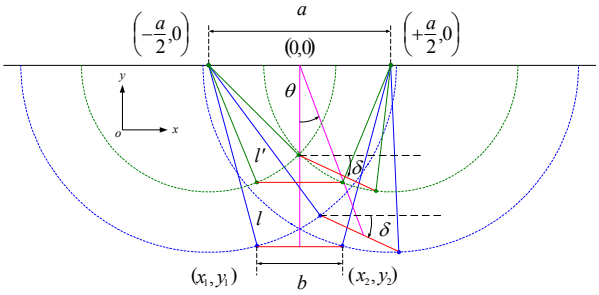

(b) The spreader inclination does not depend on rope lengths: RMQC.

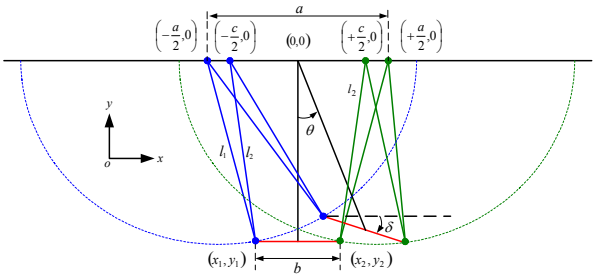

(c) RTGC (four-rope structure).

Fig. 3. Swing trajectories of the spreader: comparison of an RMQC and an RTGC.

sufficiently small and the length of the rope is constant. This gives

$$\sin\theta \approx \theta,\ \cos\theta \approx 1,\ \dot{\theta}^2 \approx 0,\ \dot{l} = \ddot{l} = 0. \quad (7)$$

If load hoisting and trolley traveling are separated, the assumption of a constant rope length can be justified. Also, in most container terminals, the occurrence of a large sway angle of the container is not permitted due to safety issues. Hence, it can be assumed that the sway angle during normal operations is small.

Then, (4)-(6) can be approximated as

$$l\ddot{\theta} + g\theta = -\ddot{x}, \quad (8)$$

$$(m_T + m_L)\ddot{x} + m_L l\ddot{\theta} = f_x, \quad (9)$$

$$m_L g - m_L \ddot{x}\theta = f_l. \quad (10)$$

This simple model provides an idea of what the input in the sway control should be. Observing (8), the control input for controlling θ is $-\ddot{x}$, which is the acceleration of the trolley. This is a fundamental fact in crane controls. Many researchers use complicated nonlinear equations or even partial differential equations as a model. But, whatever model they use, the final control law should be given as a function of the acceleration of the trolley or should be derived through the dynamics of trolley motion. Now, because (10) does not play any role in controlling θ, (10) is no longer considered. However, the maintenance of the relationship $f_l = -m_L \ddot{x}\theta + m_L g \approx m_L g$ is assumed. This suggests that the hoist motion can be decoupled from the trolley motion.

When a state feedback control is pursued, information for the entire state variables (θ, $\dot{\theta}$, x, $\dot{x}$) has to be given. If not measured, they need to be estimated. In Section 3 following, an indirect measurement of θ by measuring the inclination angle of the spreader is discussed. In Section 4, the estimations of $\dot{\theta}$ and $\dot{x}$ are discussed, whereas x is physically measured by an encoder and/or a laser sensor.

3. SWAY ANGLE MEASUREMENT

In this section, a novel method for the measurement of the sway angle of the suspended load, by measuring the inclination angle of the spreader, is presented. When compared with the use of a vision sensor, the use of an inclinometer as a sway sensor has merits in price, endurance, and maintenance.

Fig. 2(a) and Fig. 2(b) depict the individual reeving structures of an RMQC and an RTGC, respectively. Fig. 2(c) depicts a detailed drawing of the reeving structure of an RTGC. Because the lengths of the two rope-segments on the left-hand side (or right-hand side) in Fig. 2(a) are the same, it is assumed that the hoisting of the spreader in the case of an RMQC is accomplished by two ropes (see Fig. 3(a)). However, the lengths of the two rope-segments of an RTGC (see Fig. 2(b)) are different. In this case, the hoisting of the spreader is performed by four ropes (see Fig. 3(c)). Now, examining the geometry made by sheaves, ropes, and a spreader, the deviation angle of the load from the vertical line is derived.

Let θ and δ represent the sway angle of the suspended load and the inclination angle of the spreader, respectively. Let a, b, and c be the distance between the two centers of the sheaves on the trolley side, the distance between the two centers of the sheaves on the spreader side, and the diameter of the center sheave on the trolley, respectively. Note that c matters only in the RTGC case. Let l_1 and l_2 be the lengths of the outer- and inner-hoist ropes,

respectively (see Fig. 3(c)).

In the case of an RMQC, under the assumption that $a > b$, the relationship between the sway angle θ and the inclination angle of the spreader δ is derived as follows [20]:

$$\tan\theta = \frac{b\tan\delta}{-b + a\sqrt{1+\tan^2\delta}}. \quad (11)$$

It is remarked that the sway angle θ depends only on a, b, and δ, but not on the rope length *l*. Fig. 3(b) illustrates the independence of the spreader's inclination angle from the rope length. If $a = b$, the trapezoid made by *a*, *l*, and *b* becomes a parallelogram and thus the spreader does not incline. The case of $a \le b$ is excluded, because this situation would never happen in practice.

In the case of an RTGC, due to the existence of the center sheave (see Fig. 2(b)), four hoisting ropes rather than two hoisting ropes are assumed. In this case, two points, (x_1, y_1) and (x_2, y_2), do not make a circle, but each trajectory becomes an ellipse. Therefore, the following relationship is derived [20]:

$$\tan\theta = \frac{l^2}{l^2 - \left(\frac{a-c}{2}\right)^2} \cdot \frac{b\tan\delta}{-b + \frac{(a+c)}{2}\sqrt{1+\tan^2\delta}}, \quad (12)$$

where $l = (l_1 + l_2)/2$. Even though the outer-rope length l_1 and the inner-rope length l_2 vary with the swing of the spreader, the total length *l* is independent of the sway. Note that if $c = a$, (12) becomes (11). Hence, with (11) and (12), the sway angle of the spreader can be indirectly measured by measuring the inclination angle of the spreader.

4. OBSERVER DESIGN

In this section, because there is no direct way of measuring the angular velocity of the spreader, it is estimated. Note that the differentiation of the sway angle in time gives rise to noise. Various approaches to the estimation of the angular velocity are discussed. Also, the estimation problem of the linear velocity of the trolley is discussed.

4.1. Observing the sway velocity by using $\ddot{x}$

If the rope length and the acceleration of the trolley, that is, *l* and $\ddot{x}$, can be measured, (8) can be used for observing $\dot{\theta}$. Then, the observer takes the form

$$\begin{bmatrix}\dot{\hat{\theta}}\\ \ddot{\hat{\theta}}\end{bmatrix} = \begin{bmatrix}0 & 1\\ -\frac{g}{l} & 0\end{bmatrix}\begin{bmatrix}\hat{\theta}\\ \dot{\hat{\theta}}\end{bmatrix} + \begin{bmatrix}0\\ -\frac{1}{l}\end{bmatrix}\ddot{x} + \begin{bmatrix}L_1\\ L_2\end{bmatrix}(\theta - \hat{\theta}), \quad (13)$$

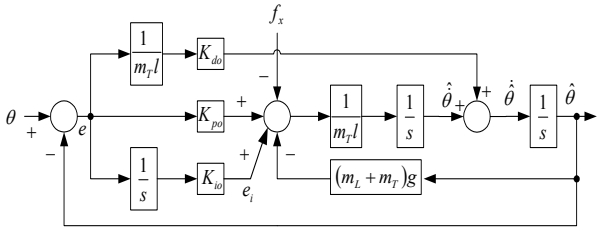

Fig. 4. Block diagram of the sway angular velocity observer.

where $\hat{\theta}$ and $\dot{\hat{\theta}}$ are the observed values of θ and $\dot{\theta}$, respectively, and L_1 and L_2 are the observer gains to be designed. Because the measurement of θ has been discussed in Section 3, only the matter of observing $\dot{\theta}$ becomes an issue here. Note that the validity of estimated results using (13) depends largely on the validity of (8). Another issue is that the measurement of *l* is normally done, but that the measurement of $\ddot{x}$ may not be practical. In this case, the methods outlined in the following subsections can be pursued.

4.2. Observing the sway velocity by using f_x

In this subsection, a method of observing $\dot{\theta}$ without using $\ddot{x}$ is discussed. If the trolley force, f_x, can be measured, (8) and (9) can be used in the observer design as follows:

$$\begin{bmatrix}\dot{\hat{\theta}}\\ \ddot{\hat{\theta}}\\ \dot{e}_i\end{bmatrix} = \begin{bmatrix}0 & 1 & 0\\ -\frac{(m_L+m_T)g}{m_T l} & 0 & \frac{1}{m_T l}\\ 0 & 0 & 0\end{bmatrix}\begin{bmatrix}\hat{\theta}\\ \dot{\hat{\theta}}\\ e_i\end{bmatrix} + \begin{bmatrix}0\\ -\frac{1}{m_T l}\\ 0\end{bmatrix} f_x + \begin{bmatrix}K_{do}/m_T l\\ K_{po}/m_T l\\ K_{io}\end{bmatrix}(\theta - \hat{\theta}), \quad (14)$$

where K_{do}, K_{po}, and K_{io} are the observer gains to be designed, and $e_i = K_{io}(\theta - \hat{\theta})/s$. A block diagram of this observer is shown in Fig. 4.

4.3. A nonlinear observer for $\dot{\theta}$

In this subsection, under the assumption that *x*, $\dot{x}$, *l*, $\dot{l}$, the trolley force f_x and the hoisting force f_l are known, a nonlinear observer for $\dot{\theta}$ using (4)-(6) is discussed. The advantage of this nonlinear observer lies in the utilization of closer system dynamics in the observer design [9,11,25]. In this subsection, a novel reduced-order nonlinear observer, motivated by the recursive design technique in [25,31], is proposed.

First, (4)-(6) are rearranged as follows:

$$\ddot{\theta} = -\frac{(2\dot{l}\dot{\theta} + g\sin\theta)}{l} - \frac{\cos\theta}{m_T l} f_x - \frac{\cos\theta\sin\theta}{m_T l} f_l,$$
$$\ddot{x} = \frac{1}{m_T} f_x + \frac{\sin\theta}{m_T} f_l,$$
$$\ddot{l} = l\dot{\theta}^2 + g\cos\theta - \frac{\sin\theta}{m_T} f_x - \frac{m_T + m_L \sin^2\theta}{m_L m_T} f_l. \tag{15}$$

Now, let $z_1 = \dot{x}$, $z_2 = \sin\theta$, and $z_3 = \dot{\theta}\cos\theta$. Then, a third-order state equation, from the first two equations of (15), is derived as follows:

$$\begin{aligned}
\dot{z}_1 &= \frac{f_l}{m_T} z_2 + \frac{1}{m_T} f_x, \\
\dot{z}_2 &= z_3, \\
\dot{z}_3 &= \cos\theta\left(-\frac{2\dot{l}\dot{\theta} + g\sin\theta}{l} - \frac{\cos\theta}{m_T l} f_x - \frac{\cos\theta\sin\theta}{m_T l} f_l \right) \\
&\quad - \dot{\theta}^2 \sin\theta \\
&= -\frac{2\dot{l}}{l} z_3 - \frac{g}{l} z_2 \sqrt{1 - {z_2}^2} + \frac{(1 - {z_2}^2)(-z_2 f_l - f_x)}{m_T l} \\
&\quad - \frac{z_2 {z_3}^2}{1 - {z_2}^2},
\end{aligned} \tag{16}$$

and

$$y = z_1.$$

Note that $z_1 = \dot{x}$ is regarded as the output of this model and that the transformation from $(\dot{x}, \theta, \dot{\theta})$ to (z_1, z_2, z_3) is invertible for all $\dot{x}$, $\dot{\theta}$ and $-\pi/2 < \theta < \pi/2$. Therefore, using (16), the state variables z_2 and z_3, that is, θ and $\dot{\theta}$, can be estimated.

The following assumptions are made: (i) $|\theta(t)|$, $|\dot{\theta}(t)|$, $|l(t)|$, and $|\dot{l}(t)|$ are bounded above by constants B_θ, $B_{\dot{\theta}}$, B_l, and $B_{\dot{l}}$, respectively, and $l(t)$ is bounded below by $b_l > 0$, for all times t; (ii) $|f_x(t)|$ and $|f_l(t)|$ are bounded above by B_{fx} and B_{fl}, respectively, and f_l is bounded below by $b_{fl} > 0$, for all times t. In fact, all of these assumptions are reasonable. The bounds are closely related to the closed-loop performance under the controller that will be designed next. However, in this subsection, the stability of the nonlinear observer will be proved under only the existence of these bounds. That is, it is enough to know the boundedness of those quantities regardless of their actual sizes. Under these assumptions, $|z_2(t)|$ and $|z_3(t)|$ are also bounded by constants $\sin(B_\theta)$ and $B_{\dot{\theta}}$, respectively.

Equation (16) can be equivalently re-written as

$$\begin{aligned}
\dot{z}_1 &= \frac{f_l}{m_T} z_2 + \frac{1}{m_T} f_x, \\
\dot{z}_2 &= z_3, \\
\dot{z}_3 &= -\frac{2\dot{l}}{l} z_3 - \frac{g}{l} z_2 \sqrt{1 - {z_2}^2} \\
&\quad + \frac{(1 - \chi_2^2(z_2))(-z_2 f_l - f_x)}{m_T l} - \frac{z_2 \chi_3^2(z_3)}{1 - \chi_2^2(z_2)} \\
&= h(z_2, z_3, l, \dot{l}, f_l, f_x),
\end{aligned} \tag{17}$$

and

$$y = z_1,$$

where $\chi_2(\cdot)$ and $\chi_3(\cdot)$ are saturation functions with saturation levels $\sin(B_\theta)$ and $B_{\dot{\theta}}$, respectively. The saturation functions were introduced in order to make the function h globally Lipschitz. This will help to find suitable observer gains. Finally, by defining new variables as

$$\begin{aligned}
\xi_2 &:= z_2 - K_2 z_1, \\
\xi_3 &:= z_3 - K_3 z_1,
\end{aligned} \tag{18}$$

where K_2 and K_3 are some constants to be designed, the following equations are obtained:

$$\begin{aligned}
\dot{\xi}_2 &= \xi_3 + K_3 y - K_2 \left(\frac{f_l}{m_T} (\xi_2 + K_2 y) + \frac{1}{m_T} f_x \right), \\
\dot{\xi}_3 &= h(\xi_2 + K_2 y, \xi_3 + K_3 y, l, \dot{l}, f_l, f_x) \\
&\quad - K_3 \left(\frac{f_l}{m_T} (\xi_2 + K_2 y) + \frac{1}{m_T} f_x \right).
\end{aligned} \tag{19}$$

Finally, the form of a reduced-order observer is just a copy of (19), as follows:

$$\begin{aligned}
\dot{\hat{\xi}}_2 &= \hat{\xi}_3 + K_3 y - K_2 \left(\frac{f_l}{m_T} (\hat{\xi}_2 + K_2 y) + \frac{1}{m_T} f_x \right), \\
\dot{\hat{\xi}}_3 &= h(\hat{\xi}_2 + K_2 y, \hat{\xi}_3 + K_3 y, l, \dot{l}, f_l, f_x) \\
&\quad - K_3 \left(\frac{f_l}{m_T} (\hat{\xi}_2 + K_2 y) + \frac{1}{m_T} f_x \right),
\end{aligned} \tag{20}$$

where

$$\hat{z}_2 = \hat{\xi}_2 + K_2 y, \quad \hat{z}_3 = \hat{\xi}_3 + K_3 y, \tag{21}$$

$$\hat{\theta} = \sin^{-1}(\hat{z}_2), \text{ and } \dot{\hat{\theta}} = \hat{z}_3 / \cos(\hat{\theta}). \tag{22}$$

To select K_2 and K_3, the error variables are defined as $e_2 := \hat{\xi}_2 - \xi_2$ and $e_3 := \hat{\xi}_3 - \xi_3$. Then, the error dynamics are obtained as follows:

$$\begin{aligned} \dot{e}_2 &= e_3 - K_2 \frac{f_l}{m_T} e_2, \\ \dot{e}_3 &= \hat{h} - \bar{h} - K_3 \frac{f_l}{m_T} e_2, \end{aligned} \tag{23}$$

where $\hat{h} = h(\hat{\xi}_2 + K_2 y,\ \hat{\xi}_3 + K_3 y,\ l,\ \dot{l},\ f_l,\ f_x)$ and $\bar{h} = h(\xi_2 + K_2 y,\ \xi_3 + K_3 y,\ l,\ \dot{l},\ f_l,\ f_x)$. Because the function h is globally Lipschitz continuous, the Lipschitz coefficient $L > 0$ can be found as follows:

$$\begin{aligned} &\left| h(\hat{\xi}_2 + K_2 y, \hat{\xi}_3 + K_3 y, l, \dot{l}, f_l, f_x) \right. \\ &\left. - h(\xi_2 + K_2 y, \xi_3 + K_3 y, l, \dot{l}, f_l, f_x) \right| \le L|e_2|^2 + L|e_3|^2 \end{aligned} \tag{24}$$

for all $\hat{\xi}_2$, $\hat{\xi}_3$, ξ_2, and ξ_3, and thus for all e_2 and e_3.

Now, in order to show the stability and convergence of the error dynamics, the following Lyapunov function candidate $V(e_2, e_3)$ is considered:

$$V(e_2, e_3) = \frac{1}{2}(e_3 - Ce_2)^2 + \frac{1}{2}e_2^2, \tag{25}$$

where $C > 0$ is a constant to be chosen. Then,

$$\begin{aligned} \dot{V} &= (e_3 - e_2)\left(\hat{h} - \bar{h} - K_3 \frac{f_l}{m_T} e_2 - C\left(e_3 - K_2 \frac{f_l}{m_T} e_2 \right) \right) \\ &\quad + e_2\left(e_3 - K_2 \frac{f_l}{m_T} e_2 \right) \\ &= (e_3 - e_2)\left(\hat{h} - \bar{h} - Ce_3\right) + e_2\left(e_3 - K_2 \frac{f_l}{m_T} e_2 \right). \end{aligned} \tag{26}$$

In (26), the second equality follows by taking $K_3 = CK_2$. Therefore,

$$\begin{aligned} \dot{V} &\le |e_3|\left|\hat{h} - \bar{h}\right| - Ce_3^2 + |Ce_2|\left|\hat{h} - \bar{h}\right| \\ &\quad + C^2|e_2||e_3| + |e_2||e_3| - K_2 \frac{f_l}{m_T} e_2^2 \\ &\le L|e_2||e_3| + Le_3^2 - Ce_3^2 + CLe_2^2 + CL|e_2||e_3| \\ &\quad + C^2|e_2||e_3| + |e_2||e_3| - K_2 \frac{f_l}{m_T} e_2^2 \\ &\le (L - C)e_3^2 + (L + CL + C^2 + 1)|e_2||e_3| \\ &\quad + (CL - K_2 \frac{b_{fl}}{m_T})e_2^2, \end{aligned} \tag{27}$$

in which $f_l(t) \ge b_{fl}$ has been used. From the above inequality, C is selected so that $C > L$, and then, K_2 is chosen sufficiently large so that $\dot{V}$ is negative except the point $e_2 = e_3 = 0$. Thereby, the uniform asymptotic stability of the observer is assured.

4.4. Observing the trolley velocity

In a typical crane system, two types of encoders are used: one is an incremental encoder and the other is an absolute encoder. In general, the incremental encoder is attached to an electric motor to measure the angular velocity of the motor, and the absolute encoder is installed in a wire-rope drum to measure the trolley/hoist velocity. Hence, there is an inherent difference between the velocity value at a motor location and the actual velocity of the trolley, because of the backlash and the elongation of the rope. Also, because a brake is installed at a motor, there is a response delay between the brake and the trolley. To overcome this problem, a Luenberger observer for estimating the trolley velocity is adopted. Therefore, the angle information from the absolute encoder is regarded as the output of the system in the observer design below.

The trolley system consists of two trolley drums, a reducer, a brake disk, and a motor rotor. Assuming that the trolley motor is connected to the trolley via a rigid coupling, the dynamics can be described as a simple two-mass model with a rigid coupling. Then, the trolley dynamics is given by

$$J_{rot} \frac{d\omega_d}{dt} = T_d - B'_d \omega_d - T_L, \tag{28}$$

where J_{rot} is the equivalent mass moment of inertia, at the trolley drum, of the entire trolley system in kg·m^2, ω_d is the angular velocity of the trolley drum in rad/sec, T_d is the torque at the trolley drum in N·m, T_L is the load torque in N·m, and B'_d is the frictional coefficient in N·m·sec/rad, which is assumed to be proportional to the angular velocity of the trolley drum. Assuming that the mechanical efficiency of the reducer is constant, the trolley drum torque T_d can be calculated using the efficiency of rotating parts η, the motor torque T_m, and the ratio of the reducer n_T as follows:

$$T_d = \eta \cdot T_m \cdot n_T, \quad \text{where } n_T = \frac{\omega_{m\_rated}}{\omega_{d\_rated}}. \tag{29}$$

In (29), ω_{m_rated} and ω_{d_rated} are the rated speeds of the trolley motor and the trolley drum, respectively.

The rotational dynamics (28) can be converted into the corresponding linear ones, using the radius of the trolley drum r_d, as follows:

$$M_{rot}\frac{dv_d}{dt} = f_m - Bv_d - f_L, \tag{30}$$

where

$$v_d = r_d\,\omega_d,\ M_{rot} = J_{rot}/r_d,$$
$$f_m = \eta \cdot T_m \cdot (n_T/r_d),\ f_L = T_L/r_d,\ B = B'_d/r_d{}^2.$$

In (30), v_d is the linear velocity of the trolley in m/sec, M_{rot} is the total equivalent mass of the trolley system at the drum in kg, f_m is the trolley force at the drum in N, and f_L is the load force in N. In addition, $df_L/dt = 0$ is assumed.

With the state vector defined by $[x_d \quad v_d \quad f_L]^T$, the system dynamics can be written in the state-space form as follows:

$$\begin{bmatrix}\dot{x}_d\\ \dot{v}_d\\ \dot{f}_L\end{bmatrix} = \begin{bmatrix}0 & 1 & 0\\ 0 & -\frac{B}{M_{rot}} & -\frac{1}{M_{rot}}\\ 0 & 0 & 0\end{bmatrix}\begin{bmatrix}x_d\\ v_d\\ f_L\end{bmatrix} + \begin{bmatrix}0\\ \frac{1}{M_{rot}}\\ 0\end{bmatrix} f_m,$$

and

$$y = \begin{bmatrix}1 & 0 & 0\end{bmatrix}\begin{bmatrix}x_d\\ v_d\\ f_L\end{bmatrix}. \tag{31}$$

Using (31), the trolley velocity observer can be constructed as follows:

$$\begin{bmatrix}\dot{\hat{x}}_d\\ \dot{\hat{v}}_d\\ \dot{\hat{f}}_L\end{bmatrix} = \begin{bmatrix}0 & 1 & 0\\ 0 & -\frac{B}{M_{rot}} & -\frac{1}{M_{rot}}\\ 0 & 0 & 0\end{bmatrix}\begin{bmatrix}\hat{x}_d\\ \hat{v}_d\\ \hat{f}_L\end{bmatrix} + \begin{bmatrix}0\\ \frac{1}{M_{rot}}\\ 0\end{bmatrix} f_m + \begin{bmatrix}L_1\\ L_2\\ L_3\end{bmatrix}(x_d - \hat{x}_d), \tag{32}$$

where L_1, L_2, and L_3 are the observer gains. A block diagram of the proposed trolley velocity observer is presented in Fig. 5. In the block disgram, $K_{dx} = L_1 M_{rot}$, $K_{px} = L_2 M_{rot}$, and $K_{ix} = -L_3$. If the three poles of the observer are all located at β,

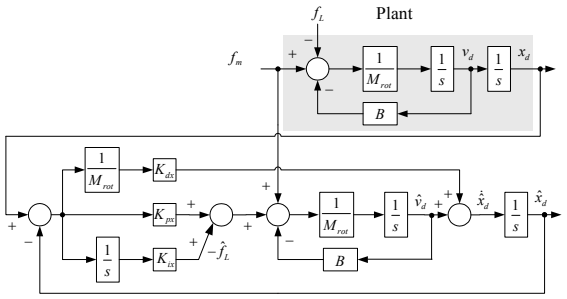

Fig. 5. Block diagram of the trolley velocity observer.

then the gains of the observer are determined as follows:

$$L_1 = -3\beta - \frac{B}{M_{rot}},$$
$$L_2 = 3\beta^2 + 3\beta\frac{B}{M_{rot}} + \left(\frac{B}{M_{rot}}\right)^2, \tag{33}$$
$$L_3 = \beta^3 M_{rot}.$$

5. CONTROL SYSTEM DESIGN

The linearized system (8) and (9) can be written in the state space form as follows:

$$\begin{aligned}\dot{\bar{x}} &= A\bar{x} + Bu,\\ y &= C\bar{x},\end{aligned} \tag{34}$$

where $\bar{x} = [x \quad \dot{x} \quad \theta \quad \dot{\theta}]^T$, $u = f_x$,

$$A = \begin{bmatrix}0 & 1 & 0 & 0\\ 0 & 0 & \frac{m_L g}{m_T} & 0\\ 0 & 0 & 0 & 1\\ 0 & 0 & -\frac{(m_T + m_L)g}{m_T l} & 0\end{bmatrix},\quad B = \begin{bmatrix}0\\ \frac{1}{m_T}\\ 0\\ -\frac{1}{m_T}\end{bmatrix},$$

and $C = \begin{bmatrix}1 & 0 & 0 & 0\\ 0 & 1 & 0 & 0\\ 0 & 0 & 1 & 0\\ 0 & 0 & 0 & 1\end{bmatrix}$.

With the formulation above, all four state variables are regarded as outputs of the system, that is, $y = [x\ \dot{x}\ \theta\ \dot{\theta}]^T$. Practically, the position of the trolley x and the sway angle θ are measured, whereas the velocity of the trolley $\dot{x}$ and the sway velocity $\dot{\theta}$ are estimated using one of the observers discussed in Section 4.

Because the state feedback control is basically a proportional control, a steady state error may exist due to model uncertainty. Therefore, to eliminate the steady state error, an integral feedback is added to the trolley position feedback x, that is, an additional

variable x_i is introduced as follows [19,26,32]:

$$\begin{aligned}\dot{\bar{x}}_a &= A_a\bar{x}_a + B_a u,\\ y &= C_a\bar{x}_a,\end{aligned} \tag{35}$$

where $\bar{x}_a = [x_i \; x \; \dot{x} \; \theta \; \dot{\theta}]^T$,

$$A_a = \begin{bmatrix} 0 & 1 & 0 & 0 & 0\\ 0 & 0 & 1 & 0 & 0\\ 0 & 0 & 0 & \frac{m_L g}{m_T} & 0\\ 0 & 0 & 0 & 0 & 1\\ 0 & 0 & 0 & -\frac{(m_T+m_L)g}{m_T l} & 0 \end{bmatrix},$$

$$B_a = \begin{bmatrix} 0\\ 0\\ \frac{1}{m_T}\\ 0\\ -\frac{1}{m_T l} \end{bmatrix}, \text{ and } C_a = \begin{bmatrix} 0 & 0 & 0 & 0 & 0\\ 0 & 1 & 0 & 0 & 0\\ 0 & 0 & 1 & 0 & 0\\ 0 & 0 & 0 & 1 & 0\\ 0 & 0 & 0 & 0 & 1 \end{bmatrix}.$$

The feedback control law is given by

$$u = f_x = -K\bar{x}_a, \tag{36}$$

where $K = [K_{ix} \;\; K_{px} \;\; K_{dx} \;\; K_{p\theta} \;\; K_{d\theta}]$. Hence, the closed loop system becomes

$$\begin{bmatrix} \dot{x}_i\\ \dot{x}\\ \ddot{x}\\ \dot{\theta}\\ \ddot{\theta} \end{bmatrix} = \begin{bmatrix} 0 & 1 & 0 & 0 & 0\\ 0 & 0 & 1 & 0 & 0\\ 0 & 0 & 0 & \frac{m_L g}{m_T} & 0\\ 0 & 0 & 0 & 0 & 1\\ 0 & 0 & 0 & -\frac{(m_T+m_L)g}{m_T l} & 0 \end{bmatrix} \begin{bmatrix} x_i\\ x\\ \dot{x}\\ \theta\\ \dot{\theta} \end{bmatrix} + \begin{bmatrix} 0\\ 0\\ \frac{1}{m_T}\\ 0\\ -\frac{1}{m_T l} \end{bmatrix} K \begin{bmatrix} x_i\\ x\\ \dot{x}\\ \theta\\ \dot{\theta} \end{bmatrix}, \quad y = \begin{bmatrix} x\\ \dot{x}\\ \theta\\ \dot{\theta} \end{bmatrix}. \tag{37}$$

Fig. 6 shows a block diagram of the state feedback controller with an integrator. The transfer functions from x_{ref} to x and from x_{ref} to θ, respectively, are given by

$$\frac{x}{x_{ref}} = \frac{ls^2+g}{ls^2+2\xi\sqrt{gl}s+g} \cdot \frac{K_{px}s+K_{ix}}{m_T s^3 + K_2 s^2 + K_1 s + K_0}, \tag{38}$$

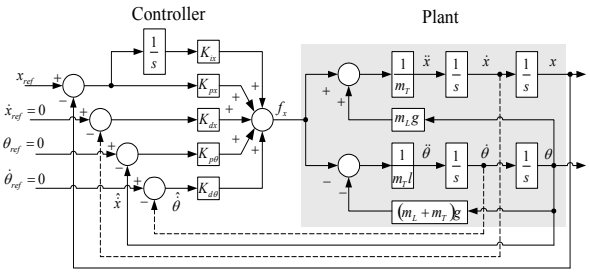

Fig. 6. A state feedback controller with an integrator.

$$\frac{\theta}{x_{ref}} = \frac{-s^2}{ls^2+2\xi\sqrt{gl}s+g} \cdot \frac{K_{px}s+K_{ix}}{m_T s^3 + K_2 s^2 + K_1 s + k_0}, \tag{39}$$

where $K_{dx} = 2\xi\sqrt{\frac{l}{g}}K_1 + K_2$, $K_{px} = 2\xi\sqrt{\frac{l}{g}}K_0 + K_1$, $K_{ix} = K_0$, $K_{p\theta} = 2\xi\sqrt{\frac{l}{g}}(lK_0 - gK_2) + gm_L$, and $K_{d\theta} = 2\xi\sqrt{\frac{l}{g}}(lK_1 - gm_T)$.

Then, the gains of the state feedback controller can be determined by determining the damping ratio ξ, K_0, K_1, and K_2. Also, K_0, K_1, and K_2 can be obtained by arranging three roots of $m_T s^3 + K_2 s^2 + K_1 s + K_0 = 0$.

On the other hand, if the closed loop poles are to be located at β_1, β_2, β_3, β_4, and β_5, the eigenvalues of $A_a - B_a K$ needs to be solved. In this case, comparing the roots of

$$\begin{aligned} &\det\left(sI - (A_a - B_a K)\right)\\ &= \det\begin{bmatrix} s & -1 & 0 & 0 & 0\\ 0 & s & -1 & 0 & 0\\ \frac{K_{ix}}{m_T} & \frac{K_{px}}{m_T} & s+\frac{K_{dx}}{m_T} & \frac{-m_L g + K_{p\theta}}{m_T} & \frac{K_{d\theta}}{m_T}\\ 0 & 0 & 0 & s & -1\\ -\frac{K_{ix}}{m_T l} & -\frac{K_{px}}{m_T l} & -\frac{K_{dx}}{m_T l} & \frac{(m_T+m_L)g - K_{p\theta}}{m_T l} & s-\frac{K_{d\theta}}{m_T l} \end{bmatrix}\\ &= s^5 + (\frac{K_{dx}l - K_{d\theta}}{m_T l})s^4 + (\frac{(m_T+m_L)g + K_{px}l - K_{p\theta}}{m_T l})s^3\\ &\quad + (\frac{K_{ix}l + K_{dx}g}{m_T l})s^2 + \frac{K_{px}g}{m_T l}s + \frac{K_{ix}g}{m_T l}\\ &= 0 \end{aligned} \tag{40}$$

with β_i, $i = 1, \cdots, 5$, the state feedback gains are given by

$$K_{ix} = \frac{m_T l \beta_1 \beta_2 \beta_3 \beta_4 \beta_5}{g},$$

$$K_{px} = \frac{m_T l(\beta_1\beta_2\beta_3\beta_4 + \beta_1\beta_2\beta_3\beta_5 + \beta_1\beta_2\beta_4\beta_5)}{g},$$

$$+\frac{m_T l(\beta_1\beta_3\beta_4\beta_5 + \beta_2\beta_3\beta_4\beta_5)}{g},$$

$$K_{dx} = -\frac{l}{g}K_{ix} + \frac{m_T l}{g}(\beta_1\beta_2\beta_3 + \beta_1\beta_2\beta_4 + \beta_1\beta_2\beta_5 + \beta_1\beta_3\beta_4 + \beta_1\beta_3\beta_5 + \beta_1\beta_4\beta_5 + \beta_2\beta_3\beta_4 + \beta_2\beta_3\beta_5 + \beta_2\beta_4\beta_5 + \beta_3\beta_4\beta_5),$$

$$K_{p\theta} = (m_T + m_L)g - m_T l(\beta_1\beta_2 + \beta_1\beta_3 + \beta_1\beta_4 + \beta_1\beta_5 + \beta_2\beta_3 + \beta_2\beta_4 + \beta_2\beta_5 + \beta_3\beta_4 + \beta_3\beta_5 + \beta_4\beta_5) + K_{px} l,$$

$$K_{d\theta} = -m_T l(\beta_1 + \beta_2 + \beta_3 + \beta_4 + \beta_5) + K_{dx} l.$$

6. EXPERIMENTATION

6.1. Pilot crane

To verify the feasibility of the proposed control scheme, a 1/4-size pilot crane of an RMQC was constructed (see Fig. 7). The natural frequency of a sway motion, ω_n, is given by $\sqrt{g/l}$. If the length of the hoist rope in the pilot crane is reduced by $1/\kappa$, where κ is the scaling factor (κ = 4 in this paper), it will not yield the same natural frequency because the gravitational acceleration g cannot be reduced by the factor of four. With the rope length reduced by κ, the sway frequency increases by $\sqrt{\kappa}$.

The time-scaling method adopted here calls for ωt to be maintained at a constant value [20,23]. Hence, the time in the pilot crane is $t/\sqrt{\kappa}$ because the natural frequency was increased by $\omega\sqrt{\kappa}$. Hence, if a velocity profile $v(t)$ is used when moving the trolley in a real crane, the profile has to be modified to $v(t)/\sqrt{\kappa}$ for use in the pilot crane. Also, if the target error range of the load is ± 20 mm in the real crane, then that in the pilot crane should be ± $20/\kappa$ mm. Similarly, if the settling time in the real crane is 10 sec, then the settling time in the pilot crane should be $10/\sqrt{\kappa}$ sec. Table 1 summarizes the scaling factors.

The reduction ratio of the pilot crane in this paper is 1:4 and hence the time-scale ratio is 1:2. Table 2 compares the key specifications between a real RMQC with those of the pilot crane. Table 3 provides the detailed specifications of the constructed pilot crane. Fig. 7 shows the side views of the pilot crane. It consists of a rope-towed trolley, a spreader, trolley rope tension adjustment bars, weight-adjustable load, and other components for hoist and trolley drives, 22 kW and 7.5 kW induction motors with inverters are utilized, respectively. The system management of the pilot crane and the implementation of the anti-sway control algorithm were carried out with a

Fig. 7. The pilot crane used in experiment: an RMQC type.

Table 1. Time scaling: a pilot crane of factor κ.

Descriptions	Real crane	Pilot crane
Hoist rope length [m]	l	l/κ
Frequency of the sway [rad]	ω	$\omega\sqrt{\kappa}$
Time [s]	t	$t/\sqrt{\kappa}$
Gravitational acceleration [m/s^2]	g	g
Velocity of the hoist and trolley [m/s]	v	$v/\sqrt{\kappa}$
Acceleration of the hoist and trolley [m/s^2]	a	a

programmable logic controller (PLC) and a DSP controller, respectively. To detect the inclination angle of the spreader, an inclinometer was installed on the top of the spreader. Finally, equation (11) has been used for the calculation of the sway angle.

6.2. Rubber tired gantry crane

It was somewhat troublesome to conduct experiments using a real RMQC and a real container ship at a port, because the ship owner does not want to lose time in accommodating an experiment. In this paper, an RTGC at the Modern Terminal in Hong Kong, designated R78, was used in verifying the performance of the proposed anti-sway system. Fig. 8(a) shows the front view of the selected R78 crane.

Table 2. Comparison of an RMQC and the pilot crane.

Descriptions	RMQC	Pilot crane
Max. length of the hoist rope [m]	29.5	12.7
Freq. of the sway [rad] / Time [s]	ω_0 / t	$2\omega_0 / 0.5t$
Hoist speed with full load [m/min]	52	26
Hoist speed w/ an empty spreader [m/min]	112	56
Trolley traveling speed [m/min]	183	91
Trolley acceleration /deceleration time [s]	5	2.5
Hoist acceleration /deceleration [m/s^2]	0.58	0.58
Trolley acceleration /deceleration [m/s^2]	0.61	0.61

Table 3. Detailed specifications of the pilot crane.

Descriptions	Value
Max. trolley travel length	13 m
Max. hoist rope length	13.36 m
Total length / height	22.695/16.23 m
Total weight of the system	40,000 kg
Max. load capability	3,115 kg
Max. hoisting speed with full load	40 m/min
Max. traveling speed	120 m/min
Trolley type	rope-towed

(a) A front view of the RTGC, R78.

(b) The head block and an inclinometer.

Fig. 8. The rubber-tired gantry crane, R78, a head block, and an inclinometer.

Table 4. General specifications of a typical RTGC.

Description	Value
Rated load	40 long ton
Weight of trolley part	32 ton
Hoisting speed with rated load (spreader only)	31 (61) m/min
Gantry travel speed with rated load (spreader only)	60 (120) m/min
Trolley travel speed	75 m/min
Engine-generator set	1 MVA

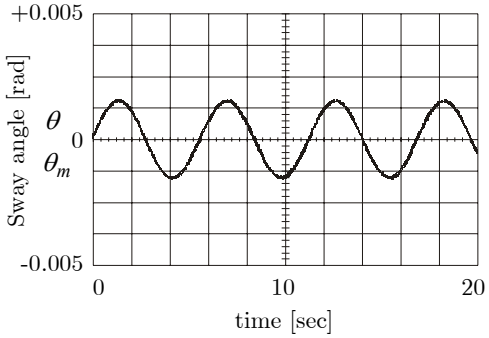

(a) For a small swing.

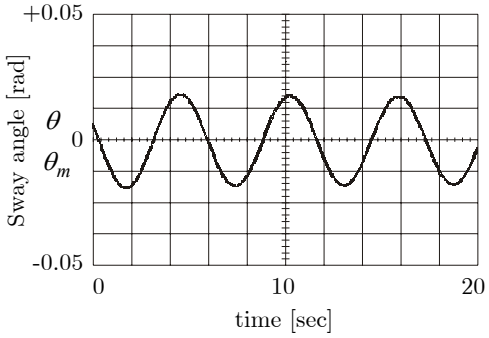

(b) For a large swing.

Fig. 9. Comparison of the sway angles (θ: vision system; θ_m: inclinometer).

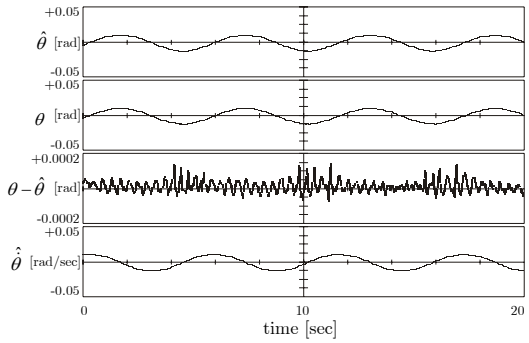

(a) For a free sway: $\theta - \hat{\theta}$ is the error between measured and estimated angles.

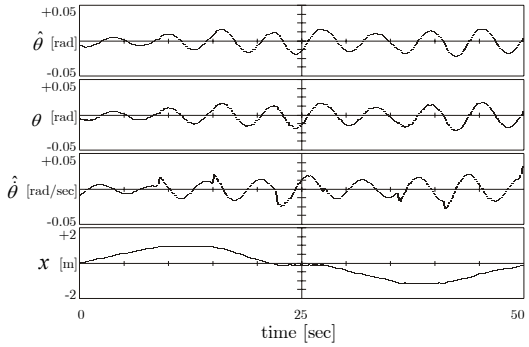

(b) For a moving trolley: x is the trolley position.

Fig. 10. Performance of the sway velocity observer ($\hat{\theta}$: the estimated sway angle; θ: the measured sway angle; $\hat{\dot{\theta}}$: the estimated angular velocity).

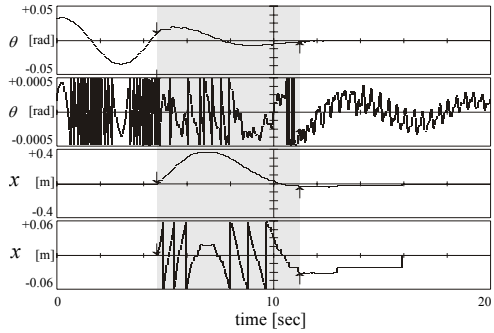

(a) Hoist rope length l = 10 m.

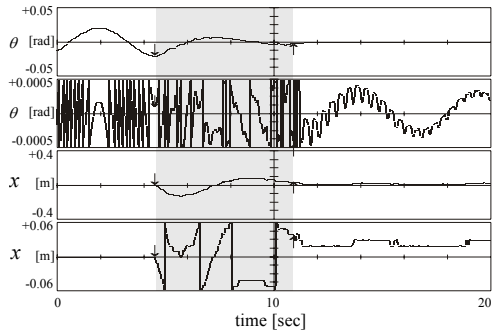

(b) Hoist rope length l = 8 m.

Fig. 11. Performance of the proposed anti-sway system in the pilot crane (from top to bottom: sway angle; magnified sway angle; trolley position; magnified trolley position).

Table 4 lists its detailed specifications. An inclinometer was installed on the top of the head block, as shown in Fig. 8(b). (12) was used for the calculation of the sway angle of the spreader. Although a DSP board controls the sway through a PLC in the pilot crane, the PLC itself in R78 controls the sway directly. All algorithms including the observers and control laws were realized using Yaskawa PLC, CP-316H. The sampling time was 10 msec.

6.3. Discussions

The experiments proceeded as follows: First, in order to verify the adequacy of the use of an inclinometer, the sway angles measured with a vision system and the calculated ones from the inclination angle of the spreader were compared. Second, the performances of the sway velocity observers were examined. Third, the performance of the proposed anti-sway control system was tested according to rope length variations.

Fig. 9 compares the experimental results of the sway angle at 8 m of rope length, where θ is the sway angle measured with a vision system and θ_m is the sway angle calculated with the measured inclination angle of the head block using an

inclinometer. As seen in Fig. 9, the difference is almost unnoticeable. This already fully justifies the use of an inclinometer. Because the distance error of the container, at a 40 m rope length, should be within

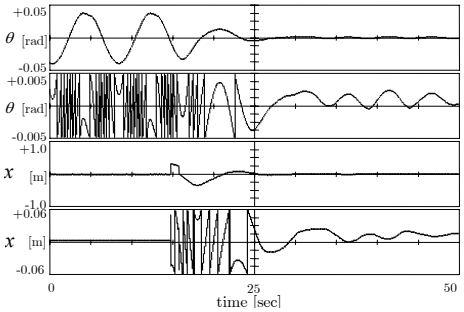

(a) l = 20 m, m_L = 12.2 ton (no container).

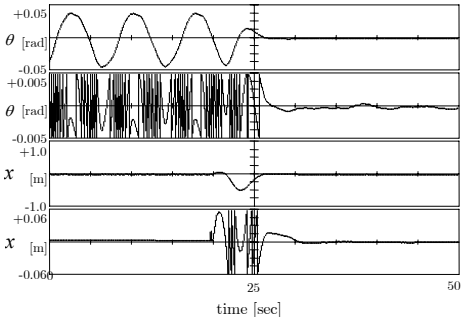

(b) l = 19.3 m, m_L = 17.2 ton (empty container).

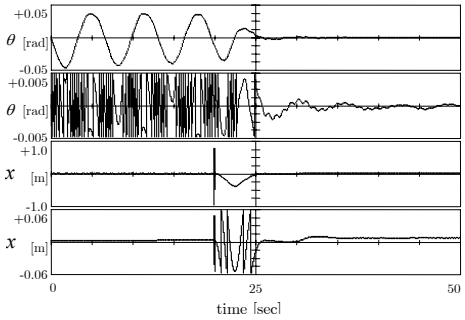

(c) l =15 m, m_L = 32.2 ton

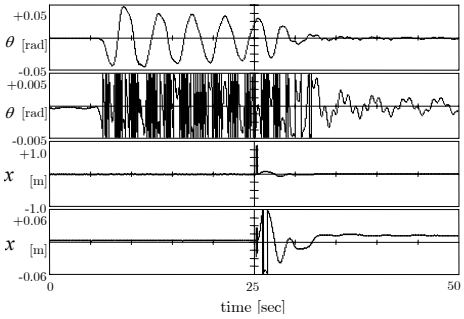

(d) l = 8 m, m_L = 42.2 ton

Fig. 12. Performance of the proposed anti-sway system with an RTGC (from top to bottom: sway angle; magnified sway angle, trolley position; magnified trolley position).

± 20 mm, ± 0.0005 rad is an acceptable error range in the sway angle. To achieve the target performance, the resolution in the measurement of the sway angle should be at least 1/5 - 1/10 of the error range.

To verify the performance of the proposed sway velocity observer, further experiments were carried out. First, the performance under the free sway of the suspended load was tested. Second, the performance with a moving trolley was verified. The hoist rope length used was 8 m. As shown in Fig. 10(a), the estimation error of the sway angle is within ± 0.0002 rad, which is within the target error range. Also, for a moving trolley, the observer estimates the sway velocity well enough, as shown in Fig. 10(b).

To prove the performance of the proposed anti-sway control system, the system was tested at the pilot crane with rope lengths of 10 m and 8 m, respectively. The required error ranges should be within ± 0.0005 rad in the sway angle and ± 0.03 m at the trolley position. The experimental results in Fig. 11 demonstrate that the proposed control system satisfies all the target ranges well.

6.4. RTGC

To verify the feasibility of the application of the proposed anti-sway system to a real RTGC, the algorithm was tested under various rope-length conditions and load weights in a container terminal in Hong Kong. Fig. 12(a) shows the experimental results under l = 20 m and no load. Fig. 12(b) shows the results under l = 19.3 m and an empty container. The weight of the empty container is 5 tons. The weight of the head block and the spreader is 12.2 tons. Therefore, the weight of the load is 17.2 tons. Fig. 12(c) shows the performance under l = 15 m and m_L = 32.2 tons. For l = 8 m and m_L = 42.2 tons, the results are as shown in Fig. 12(d). The target performance of this crane is that the error of the sway angle be within ± 0.0025 rad, which corresponds to the 0.05 m deviation of the load at l = 20 m, and theerror of the trolley position is within ± 0.03 m. As shown in Fig. 12(a-d), the proposed control system satisfies all target performances.

7. CONCLUSIONS

In this paper, the sway control problem of container cranes with multiple ropes was investigated, whereas a single-rope pendulum structure has been used in the literature. Using the kinematics of the hoist reeving mechanism, a new sway-angle detection method using the inclinometer attached on the head block was proposed. The proposed method, compared with the results obtained by using a vision sensor, showed almost the same performance, but with a much reduced cost. To suppress the sway, a multivariable state feedback controller with an integrator was

proposed. To verify the feasibility of the proposed control system, a 1/4-size rail-mounted quayside pilot crane was built. The performance of the proposed system was synthetically verified with the pilot crane. Also, experiments with a real rubber-tired gantry crane in Modern Terminal, Hong Kong, were carried out. The developed sway-angle measurement method and control algorithm are simple but are very cost-effective and promising.

REFERENCES

[1] B. d'Andrea-Novel and J. M. Coron, "Exponential stabilization of an overhead crane with flexible cable via a back-stepping approach," *Automatica*, vol. 36, pp. 587-593, 2000.

[2] J. W. Auernig and H. Troger, "Time optimal control of overhead cranes with hoisting of the load," *Automatica*, vol. 23, no. 4, pp. 437-447, 1987.

[3] G. Bartolini, A. Pisano, and E. Usai, "Second-order sliding-mode control of container cranes," *Automatica*, vol. 38, no. 10, pp. 1783-1790, 2002.

[4] F. Boustany and B. d'Andrea-Novel, "Adaptive control of non-completely controlled mechanical systems using dynamic feedback linearization and estimation design," *Int. J. Adaptive Control and Signal Processing*, vol. 6, pp. 589-610, 1992.

[5] C.-C. Cheng and C.-Y. Chen, "Controller design for an overhead crane system with uncertainty," *Control Engineering Practice*, vol. 4, no. 5, pp. 645-653, 1996.

[6] C. C. Chung and J. Hauser, "Nonlinear control of a swinging pendulum," *Automatica*, vol. 31, no. 6, pp. 851-862, 1995.

[7] G. Corriga, A. Giua, and G. Usai, "An implicit gain-scheduling controller for cranes," *IEEE Transactions on Control Systems Technology*, vol. 6, no. 1, pp. 15-20, 1998.

[8] Y. Fang, W. E. Dixon, D. M. Dauson, and E. Zergeroglu, "Nonlinear coupling control laws for an underactuated overhead crane system," *IEEE/ASME Trans. on Mechatronics*, vol. 8, no. 3, pp. 418-423, 2003.

[9] J. P. Gauthier, H. Hammouri, and S. Othman, "A simple observer for nonlinear systems: applications to bioreactors," *IEEE Trans. Automat. Contr.*, vol. 37, no. 6, pp. 875-880, 1992.

[10] General Electric Company, "Electronic anti-sway control," US patent number 5443566, 1995.

[11] A. Giua, M. Sanna, and C. Seatzu, "Observer-controller design for three dimensional overhead cranes using time-scaling," *Mathematical and Computer Modeling of Dynamical Systems*, vol. 7, no. 1, pp. 77-107, 2001.

[12] J. J. Hamalainen, A. Marttinen, L. Baharova, and J. Virkkunen, "Optimal path planning for a trolley crane: fast and smooth transfer of load," *IEE Proc. Control Theory Appl.*, vol. 142, no. 1, pp. 51-57, 1995.

[13] K. S. Hong, S. C. Sohn, and M. H. Lee, "Sway control of a container crane (part I): modeling, control strategy, error feedback control via reference velocity profiles," *Journal of Control, Automation and Systems Engineering* (in Korean), vol. 3, no. 1, pp. 23-31, 1997.

[14] K. S. Hong, S. C. Sohn, and M. H. Lee, "Sway control of a container crane (part II): regulation of the pendulum motion through patternizing the trolley moving velocity," *Journal of Control, Automation and Systems Engineering* (in Korean), vol. 3, no. 2, pp. 132-138, 1997.

[15] K. S. Hong, "Container crane control: modified time-optimal traveling followed by nonlinear residual sway control," *Journal of Control, Automation, and Systems Engineering* (in Korean), vol. 5, no. 5, pp. 630-639, 1999.

[16] K. S. Hong, B. J. Park, and M. H. Lee, "Two-stage control for container cranes," *JSME International Journal, Series C*, vol. 43, no. 2, pp. 273-282, 2000.

[17] K. T. Hong, C. D. Huh, and K. S. Hong, "Command shaping control for limiting the transient sway angle of crane systems," *International Journal of Control, Automation, and Systems*, vol. 1, no. 1, pp. 43-53, 2003.

[18] K. S. Hong, C. W. Kim, and K. T. Hong, "Boundary control of an axially moving belt system in thin-metal production line," *International Journal of Control, Automation, and Systems*, vol. 2, no. 1, pp. 55-67, 2004.

[19] Y. S. Kim, H. Seo, and S. K. Sul, "A new anti-sway control scheme for trolley crane system," *36th IEEE Conf. on Industry Applications*, pp. 548-552, 2001.

[20] Y. S. Kim, *Control Systems for Suppressing Sway of a Suspended Load without a Vision System*, Ph.D. Dissertation, School of Electrical Engineering, Seoul National University, 2002.

[21] Y. B. Kim and Y. G. Jung, "A study of the sway control of a container crane based on H-infinity gain-scheduling approach," *Journal of Control, Automation, and Systems Engineering* (in Korean), vol. 7, no. 7, pp. 559-566, 2001.

[22] G. A. Manson, *Time Optimal Control Methods Arising from the Study of Overhead Cranes,* Ph.D. thesis, University of Strathclyde, Glasgow, U.K., 1977.

[23] A. Marttinen, J. Virkkunen, and R. T. Salminen, "Control study with a pilot crane," *IEEE Trans. on Education*, vol. 33, no. 3, pp. 298-305, 1990.

[24] K. A. F. Moustafa and A. M. Ebeid, "Nonlinear

modeling and control of overhead crane load sway," *Journal of Dynamic Systems, Measurement, and Control*, vol. 110, pp. 266-271, 1988.
[25] H. Nijmeijer and T. I. Fossen, *New Directions in Nonlinear Observer Design*, Springer-Verlag, 1999.
[26] B. S. Park and J. S. Yoon, "A design of model-following time delay controller with modified error feedback controller," *Journal of the Korean Society of Precision Engineering* (in Korean), vol. 17, no. 12, pp. 176-184, 2000.
[27] U. H. Park, J. W. Lee, and S. H. Noh, "Reduction of residual vibration for 2 axes overhead crane by input shaping," *Journal of the Korean Society of Precision Engineering* (in Korean), vol. 17, no. 4, pp. 181-188, 2000.
[28] Y. Sakawa and Y. Shindo, "Optimal control of container cranes," *Automatica*, vol. 18, no. 3, pp. 257-266, 1982.
[29] Y. Sakawa and H. Sano, "Nonlinear model and linear robust control of overhead traveling cranes," *Nonlinear Analysis, Theory, Methods & Applications*, vol. 30, no. 4, pp. 2197-2207, 1997.
[30] W. Singhose, L. Porter, M. Kenison, and E. Kriikku, "Effects of hoisting on the input shaping control of gantry cranes," *Control Engineering Practice*, vol. 8, no. 10, pp. 1159-1165, 2000.
[31] H. Shim and J. H. Seo, "Recursive observer design beyond the uniform observability," *39th IEEE Conf. on Dec. and Control*, pp. 809-814, 2000.
[32] H. W. Smith and E. J. Davison, "Design of industrial regulators: Integral feedback and feedforward control," *IEE Proc.*, vol. 119, no.8, pp. 1210-1216, 1972.
[33] J. S. Yoon and E. S. Kang, "A study on the anti-swing and position controller for overhead cranes," *Trans. Korean Society of Mechanical Engineers* (in Korean), vol. 19, no. 6, pp. 1391-1401, 1995.

Yong-Seok Kim received the B.S., M.S., and Ph.D. degrees in Electrical Engineering from Seoul National University, Seoul, Korea, in 1996, 1998, and 2002 respectively. He was with the Korea Electrical Engineering and Science Research Institute as a Research Engineer from 2002 to 2003. Since 2003, he has been with HMC (Hyundai Motor Company) as Senior Research Engineer. In HMC, he has worked on the development of the control algorithm for HCU (Hybrid electric vehicle Control Unit) and MCU (Motor Control Unit). His research interests include control of hybrid electric vehicles and high performance control of electro-mechanical system using power electronics.

Keum-Shik Hong received the B.S. degree in Mechanical Design and Production Engineering from Seoul National University in 1979, the M.S. degree in Mechanical Engineering from Columbia University, New York, in 1987, and both the M.S. degree in Applied Mathematics and the Ph.D. degree in Mechanical Engineering from the University of Illinois at Urbana-Champaign in 1991. Since Dr. Hong joined the School of Mechanical Engineering at Pusan National University, Korea, in 1993, he is now Professor. During 1982-85, he was with Daewoo Heavy Industries, Incheon, Korea, where he worked on vibration, noise, and emission problems of vehicles and engines. Dr. Hong serves as Associate Editor for Automatica (2000-date) and as Editor for the International Journal of Control, Automation, and Systems (2003-date). He also serves as Associate Editor in IEEE and IFAC conferences editorial boards. Dr. Hong received Fumio Harashima Mechatronics Award in 2003. He is a member of ASME, IEEE, ICASE, KSME, KSPE, KIEE, and KINPR. Dr. Hong's current research interests include nonlinear systems theory, adaptive control, distributed parameter system control, input shaping, vehicle control, and innovative control applications to engineering problems.

Seung-Ki Sul received the B.S., M.S., and Ph.D. degrees in Electrical Engineering from Seoul National University, Korea, in 1980, 1983 and 1986, respectively. From 1986 to 1988, Dr. Sul was with the Department of Electrical and Computer Engineering at University of Wisconsin-Madison as Associate Researcher. After that, he joined Gold-Star Industrial Systems Company as Principal Research Engineer from 1988 to 1990. Since 1991, he has been a faculty of the School of Electrical Engineering at Seoul National University, and now is Professor. Dr. Sul spent his sabbatical year in Yaskawa Electric Corporation as a R&D adviser from 2003 to 2004. His current research interests include power electronic control of electric machines, electric vehicle drives, and power converter circuits.